Creating a Dynamic Periodic Poling System for X-Cut Lithium Niobate Chip-Scale Integrated Optics

Undergraduate Honors Thesis

Presented in Partial Fulfillment of the Requirements for Graduation with Honors Research Distinction in Electrical and Computer Engineering at The Ohio State University

By

Andrew Havre Phillips

May 2016

The Ohio State University

Department of Electrical and Computer Engineering

Advisor: Dr. Ronald M. Reano

Abstract

A system for periodically poling x-cut lithium niobate (LN) is designed and tested. LabVIEW was used for instrumentation control software to create and send an arbitrary waveform to an arbitrary waveform generator and then into a high-voltage amplifier. This high-voltage waveform was then applied through a designed poling circuit and sample station onto the prepared LN sample. Both the LabVIEW software and the poling circuit were designed to be easy to use and dynamic to allow for the poling of multiple different materials.

The baseline poling of LN was achieved using the LabVIEW software and poling setup. The poling was characterized using FIB milling and HF etching, as well as with piezoresponse force microscopy (PFM). Although it could be optimized, the PFM did show successful poling in a non-destructive way. MgO-doped LN (MgO:LN) was then attempted, but no poling results were achieved.

Overall, the poling system was successful in baseline poling x-cut LN for on-chip integrated optics and in laying the foundation for poling other materials, as well. Future work includes decreasing the effects of leakage current in poling MgO:LN and investigating the possibilities of reverse poling and thin film poling.

Acknowledgements

Firstly, I want to thank Dr. Ronald Reano for giving me the opportunity to reach into the unknown of research and get something out of it. His mentorship and guidance have been invaluable as I transition into a graduate student, and his philosophies are inspiring.

I also want to thank Tyler Nagy for allowing me to work with him on this part of his project. He has introduced me to working in a lab environment and has taught me multiple practical skills. I thank him for using the e-beam, doing the FIB milling and HF etching, and spending many hours with me conducting poling tests. I appreciate his creative ideas and constant preparation for things to take longer than expected.

Lastly, I want to thank Michael Wood for his manufacturing and characterization processes expertise. Without his willingness to work and teach, I would not have any results to show at all.

This research is also partially supported by the College of Engineering Undergraduate Research Scholarship.

Table of Contents

List of Figures

List of Tables

1. Introduction

1.1 Background and Motivation

Nonlinear optics is the study of the interaction of laser light with optical materials [1]. The associated processes are nonlinear in that the input light wavelength and the output light wavelength are different and the output light wavelength depends on the input. Different materials have different nonlinear optical properties which can create different processes. One common example of a nonlinear optical process is second-harmonic generation (SHG). SHG is the doubling of an input light frequency as it passes through a second-order nonlinear optical material. A schematic of SHG is shown below in Figure 1. There are many other similar processes, such as sum-frequency generation (SFG), difference-frequency generation (DFG), and third-harmonic generation (THG). These are the building blocks of nonlinear optical systems. There is a wide range of applications for these nonlinear optical processes and materials such as: high speed telecommunications, chemical sensors, and green and blue laser light generation. In particular, there is now a drive for integrating nonlinear optical systems on photonic chips, which can impact other fields, as well. For example, integrated optical chips can use concentrated high-intensity light as very sensitive sensors to detect what disease exists in a sample of blood through molecular fingerprinting for a biomedical engineering problem.

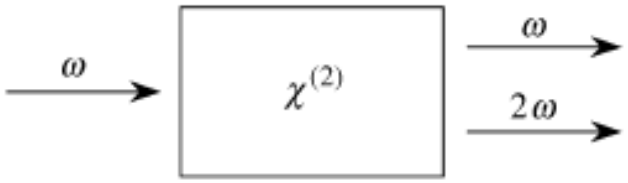

Figure 1: Schematic of second-harmonic generation (SHG) showing an input wave of frequency ω and two output waves of frequencies ω and 2ω. The symbol in the box represents second-order nonlinear properties. [1]

Although these effects are powerful, there are hindrances. All materials experience some degree of dispersion. Being dispersive means that the speed at which light travels through the material is a function of its frequency. This means that light beams of different frequencies travel at different speeds and become out of phase with each other [2]. The efficiency of any nonlinear optical process decreases to almost zero when there is a lot of phase mismatch among the interacting light beams. There are generally two methods used for improving phase mismatch and increasing efficiency: birefringent phase matching and quasi-phase matching.

One widely exploited crystal is lithium niobate ($LiNbO_3$ or LN) because it has large electro-optical and nonlinear optical coefficients [3] and is easy to repeatedly fabricate for optical waveguide use [4]. The traditional method of birefringent phase matching has large temperature dependencies and requires waves to be polarized in perpendicular directions. However, the largest nonlinear coefficient for $LiNbO_3$ occurs when the waves are all polarized in the z-direction (d_{ss} coefficient) [4]. So, birefringent phase matching is not convenient for use with $LiNbO_3$, and another method is used.

Quasi-phase matching (QPM) is a process for changing the spontaneous polarization in a ferroelectric crystal in a periodic manner to "correct" this phase mismatch [2]. Figure 2 on the next page shows that while QPM cannot reach maximum efficiency, it can greatly increase the ability of a material like $LiNbO_3$ to produce SHG, for example. Periodic poling is the process of reversing the polarizations of a crystal by applying a large electric field [4]. The required strength of the electric field to reverse the poles is called the coercive strength of the material, and for $LiNbO_3$, it is about 21 kV/mm [2]. For certain materials like $LiNbO_3$, these reversals remain after the application of the electric field due to the piezoelectric effect. Piezoelectric materials have the property that an applied electric field can cause the electrons to move and

physically change the polarity of the material. Figure 3 shows schematically the results of periodically poling a material.

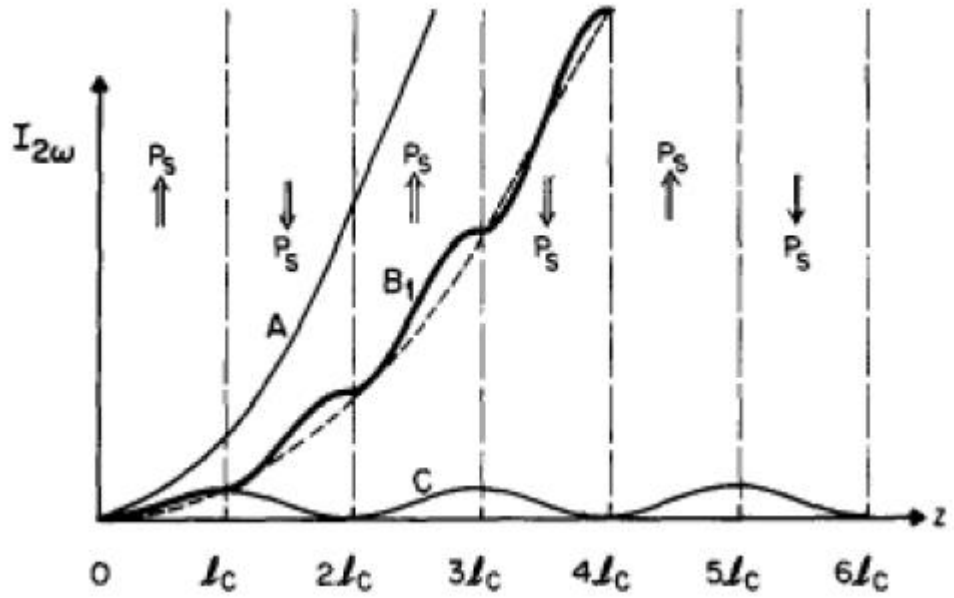

Figure 2: Plot showing the effect of quasi-phase matching on the intensity (efficiency) of the nonlinear optical process. Curve A shows perfect phase matching and the best efficiency. Curve B shows quasi-phase matching and moderate efficiency. Curve C shows no phase matching and very low efficiency. [2]

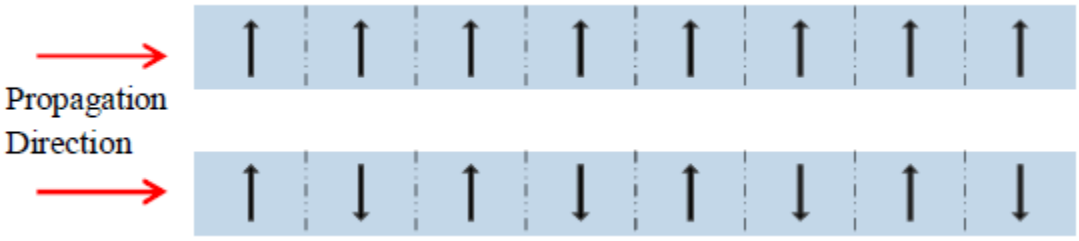

Figure 3: Schematic showing the polarizations of a material before (top) and after (bottom) being poled. The after image shows periodic domain inversions which serve to correct the optical process every so often. [2]

The process of periodically poling a material involves placing electrodes on the material in such a way to be able to apply a high-voltage pulse in the proper direction across the material. Electrodes are commonly deposited onto the material by processes such as lift-off or lithography.

They are designed to direct the applied electric fields in strips across the material to pole at a certain duty cycle (often 50%). There are many conventional poling waveforms, but they all have in common the idea of rising just above the coercive voltage needed to switch the material's polarizations. Also, a material can be x-cut or z-cut to be poled, and there are different setups depending on the direction. Z-cut poling is the most prevalent historically and involves putting a positive electrode on top (+Z face) and a negative or ground electrode on bottom (-Z face) of a sample. This makes the thickness of the sample the poling distance. However, the other option is x-cut or y-cut poling, which involves placing both electrodes on the same face and switching polarizations along the x- or y-axis. This planar poling method is more practical for use for integrated photonics [5].

1.2 Objectives

The first objective is to create a basic poling system and achieve baseline poling of x-cut LN per normal operations similar to those outlined in the literature. This involves designing and implementing arbitrary waveform control software to send a desired waveform as well as circuitry to allow for proper poling and measurements.

Once baseline poling is achieved, the second objective is to pursue the poling of materials with different properties, such as MgO-doped LN (MgO:LN). This involves improving the baseline poling system to be able to adapt to poling other materials.

The results and components of the dynamic poling system are presented.

2. Poling Setup and Circuit Design

2.1 Experimental Setup and Equipment

The poling setup needed to have a way of applying an arbitrary waveform of the correct voltage to a small sample and give feedback to the user during poling. The setup design described here has three main parts: the control cart, the poling circuit, and the sample station. A high level block diagram of the components and their inputs and outputs is Figure 4 below. A list of the parts used in the poling setup is in Table A1 in Appendix A, Poling Setup Materials.

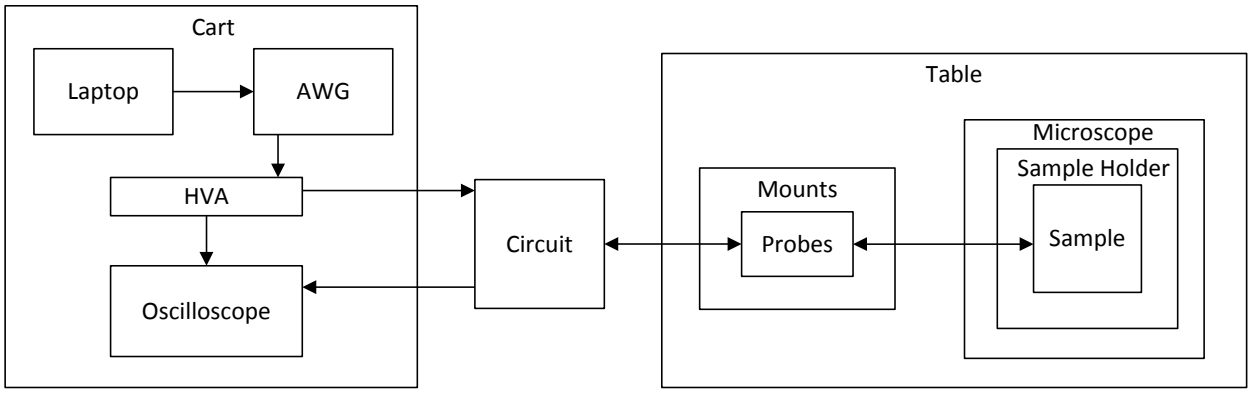

Figure 4: High level bock diagram of poling setup and equipment. The arrows represent physical connections in the form of wires and cables and inputs and output directions.

The control cart includes all of the software and input devices for the user to use. The SRS DS345 Arbitrary Waveform Generator (AWG) and the Trek 20/20C High-Voltage Amplifier (HVA) were two main components. The AWG is used for generating arbitrary poling waveforms and sending them at the right time. The HVA is used to amplify the waveform to the correct poling voltages. The Trek HVA used has a gain of 2000 V/V. Since the HVA has the ability to amplify output voltages to levels dangerous to humans, it was important that the Trek 20/20C manual [6] specified its classification as overvoltage categories I and II of the EN 61010-

1 voltage safety standards. These categories relate to being able to use the instrument at the peripheral level and the local level, such as connecting to the wall outlet. The EN 61010-1 safety standards ensure that the hazard level of things like electric shock, burn, and high temperatures are minimal. The specific AWG and HVA instruments were chosen because they are mentioned in the literature as being used in other similar poling experiments [4, 7]. In addition, an HP Infinium Oscilloscope is used to provide feedback during the poling process. The oscilloscope measures certain voltages from the circuit and displays them in real-time, so, it is easy to know if the poling is working. Also on the control cart is the laptop which is connected to the AWG. The laptop runs LabVIEW software to create, send, and trigger the waveform on the AWG output. This software is discussed more in Section 3. Overall, having all of this equipment on one cart is convenient for control and for movement. Figure B1 in Appendix B, Poling Setup Pictures, shows the control cart with all of the instruments.

The sample station is on a table near the control cart and includes the probes and sample holder. The DC probes are connected back to the poling circuit and then to the two electrodes on the sample. One feature of the probes is that their base is magnetic. Mounts and mount brackets were obtained to elevate and secure the probes, and a custom-made steel stand was added for each probe to allow some analog movement of the base. Then, the magnetic base lock can be activated to secure the probes to the steel stands. Also, in order to see the electrodes and make sure the probe tips contact the correct part, the sample is located on an elevated microscope stand. This microscope also has a camera function for taking images of the electrodes and probe placements. The LN sample itself is held down in a small wafer holder with four little clips and screws. Figure B2 and Figure B3 in Appendix B, Poling Setup Pictures, show the sample station as a whole and a close-up on the sample holder, respectively.

In between the control cart and the sample station is the poling circuit. This circuit has specific resistors to control the parameters of the poling and measurement, and its design is the subject of Section 2.2. Connecting the control cart to the circuit are the HVA cable and the oscilloscope 10:1 measurement probes. Then, the voltages on each side of the sample are sent from the circuit through triaxial cables and adapters to the DC probes. Figure B4 in Appendix B, Poling Setup Pictures, shows the poling circuit box with input and output jacks and measurement wires.

2.2 Poling Circuit

The basic poling circuit setup matched across multiple poling research papers [8, 9]. Figure 5 below is a picture of the used poling circuit showing the resistors, the sample, and the oscilloscope probe locations.

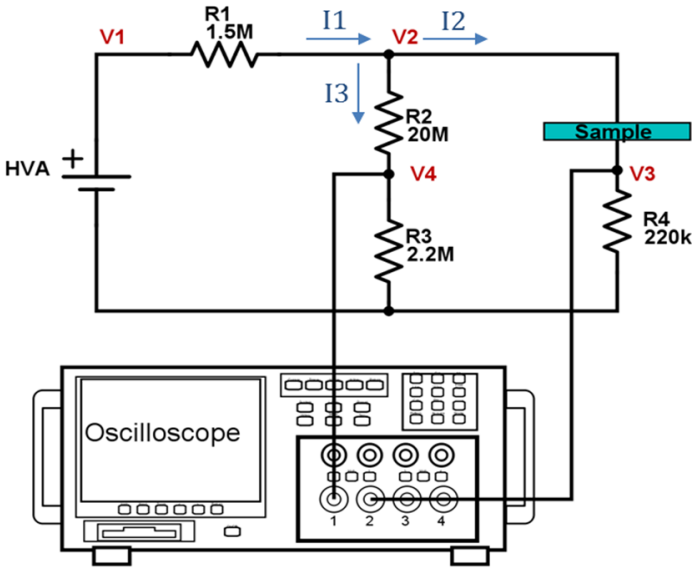

Figure 5: Poling circuit schematic showing the sample and oscilloscope probe locations, as well.

Designing the circuit involved choosing the appropriate resistor values for the poling process. In the figure above, R1 affects the voltage across the sample, R4 affects poling current and the magnitude of V3 measured, and R2 and R3 act as a voltage divider to indirectly measure the high voltage across the sample.

To select appropriate resistor values, a MATLAB Poling Analysis script was made to be able to quickly tune the values. The KVL circuit analysis was done for the circuit, and the resistance of the oscilloscope probes was included. This MATLAB script is in Appendix C, MATLAB Code. It includes code for normal operation of poling, the open circuit case, and the short circuit case. For the LN sample, the chosen resistor values are seen in the figure above. These values give a theoretical poling current of about 15 uA and an input pulse of about 1 second. The ideal V3 is on the order of 10 V.

The limiting factor on the resistor choices was that the resistors were all eighth-Watt resistors. So, the calculated current had to be small enough to not surpass the resistor power rating.

3. Poling Software and Waveform Design

3.1 LabVIEW Control Software

In order to control the SRS DS345 arbitrary waveform generator (AWG) to properly send the poling waveform, software was used on a connected laptop. The DS345 has associated software called the Arbitrary Waveform Composer (AWC) [10]. The AWC software allows for creating and downloading waveforms to the AWG via RS232 or GPIB connections. However, the main disadvantage of using the AWC is that it requires the user to build waveforms by adding and subtracting pieces of other basic waveforms step by step. This was seen to take too

much time to create the types of waveforms needed for poling. Thus, there was a need to design new software to control the AWG and poling process.

The main requirements of the poling software were that the user be able to easily create waveforms composed of linear parts and be able to edit the voltages and durations individually. Additionally, the user needed to be able to see the waveform generated in real time, and send and trigger the waveform on the AWG with simple button clicks. LabVIEW was chosen as the programming language because it is often used for instrumentation control and timing, and there were other systems in the lab running LabVIEW. So, to promote coherence in the lab and the ability to properly control the instruments, the AWG control software was designed in LabVIEW.

The LabVIEW software communicates with the AWG over general purpose interface bus (GPIB), a common industry communication protocol for instruments and microcontrollers. The AWG manual [11] lists the GPIB commands used to control it via software. In order to use these commands, the industry standards of how to send data over GPIB and how to control its timing were investigated.

Commands for the AWG are sent as text phrases and arguments which the AWG can recognize. In LabVIEW, these commands are easily represented as character strings separated by delimiters. There are GPIB Read and Write VIs created for receiving and sending commands and data. Once the AWG has been notified that the arbitrary waveform data is ready to be transmitted, it will accept the data over GPIB in 16 bit binary form. Since binary can only represent integers, the precision of actual floating point voltages is achieved by mapping the range of possible floating point voltages to the range of binary values. While there is still some truncation, the step size is small enough to be able to send data in 0.003 V increments, which is

plenty precise for this purpose. The timing for sending commands and data and receiving ready signals in the LabVIEW code is handled by adjusting the timeouts of the Read and Write VIs. By allowing the functions more or less time to complete the tasks before timing out, the code can make sure that each task is completed before the next command is sent. Failure to properly control the timing when sending so many commands results in an error on the AWG.

The general process of designing this code followed the introduction and testing of commands and features individually. For example, the user interface and method for creating the waveforms were designed first. This front-end functionality was tested. Then, some of the GPIB commands for testing the AWG and setting parameters like the amplitude and sampling frequency were included. Once the AWG successfully accepted the commands and changed its parameters, the code for sending the waveform data was made. This part of the code is the most complicated and involves lots of careful timing. At this point in the design process, the AWG output was connected to the oscilloscope to verify the waveform created in the user interface could reach the oscilloscope correctly.

After much testing with the oscilloscope, adjusting the timing levels, and adding in new features, the LabVIEW poling software was completed. The final version of the front panel, or user interface, is seen on the next page as Figure 6. The backend of the code, the block diagram, is shown in pieces in Appendix D, LabVIEW Code.

This LabVIEW software has many features and strengths in its design. Waveform creation involves inputting the start voltage, end voltage, and segment duration for each linear part into the table in the middle. This allows the user to easily add or remove segments and edit their voltage and durations easily. As the user types data in the table, the waveform appears on the graph on the right for verification. The amplitude scaling input box allows the user to

multiply the waveform described in the table by a constant. This updates the graph but leaves the table as the user inputted. The advantage of this for poling is that just one standard poling waveform can be created, and then the amplitude scaling feature can be used to change the poling voltage for testing or for different materials. If the peak-to-peak voltage of the created waveform exceeds the limit of the AWG, the Vpp error LED will turn on.

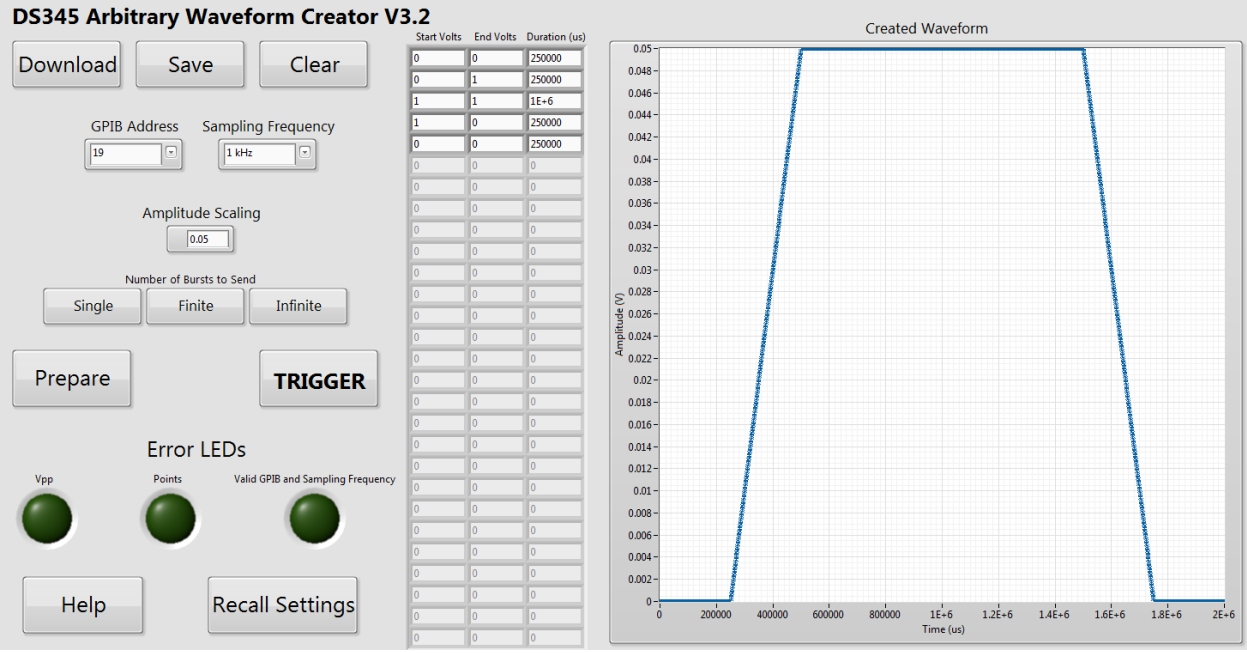

Figure 6: Final working version of the user interface for the LabVIEW poling software.

The sampling frequency of the waveform can be selected, and that affects the waveform's point density. Only frequencies which the AWG can accept are selectable. Point density is shown visually by visible points on the waveform graph. The higher density of points, the more precisely the waveform can change voltages. However, as the sampling frequency increases for a given pulse length, the number of points increases. This can reach the upper limit of the number

of data points the AWG can handle. So, an error checking LED for points was added to tell the user when the waveform has too many or too few points.

The download and save buttons at the top allow for the user to create a waveform only once, save it as a formatted text file, and then be able to download it later without typing in the voltages again. The clear button allows for easy restarting of the inputted waveform.

The help button at the bottom opens up a PDF manual for how to use the software. The recall settings button is a fail-safe to automatically readjust the AWG settings to those required for poling in case it gets off somehow.

Finally, the most important buttons are the prepare and trigger buttons in the middle left of the user interface. Once the user has created the desired waveform, the prepare button will send the commands to the AWG to set its parameters, tell it that the waveform data is ready, and then load the waveform data onto the AWG. Upon successful completion, the AWG will display "Load Done". After this, the user only needs to press the trigger button to trigger the AWG to output the loaded arbitrary waveform. An advantage of this trigger functionality is that the AWG will not output anything until the trigger button is pressed. This keeps the system at a safe and steady voltage of zero until the user is ready to send the pulse and to pole.

3.2 Poling Waveform

Literature shows many similar kinds of conventional poling waveforms [4, 8, 9, 12, 13]. They all have in common the rise to just above the coercive field voltage in order to cause the domains to switch. For the purposes of achieving baseline poling, the simple waveform shown in Figure 7 on the next page was used.

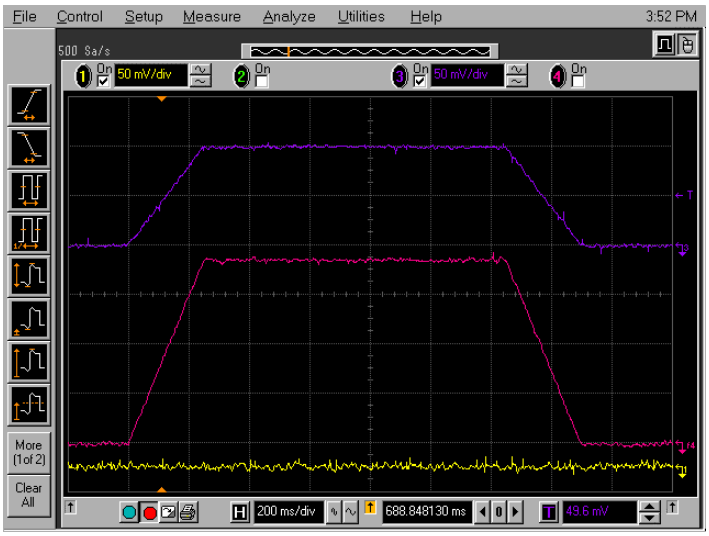

Figure 7: Normal input poling waveform used for basic poling experiments. The purple line is the input waveform, and with the 2000 V/V gain of the HVA, it has a peak of 200 V here.

In designing the applied waveform, there are two main variables: the peak voltage and the duration of this peak voltage. The peak voltage is chosen as something just greater than the coercive field voltage. For the LN samples, the electrode gap was 10 um. So, with a coercive field of 21 kV/mm, the coercive field voltage for this electrode setup is about 210 V. So, the applied peak pulse voltage was chosen to be 250 V to be well over the required voltage.

Determining the pulse length requires more calculation. It is based on the charge and current required for the poling as:

$$Pulse\ length\ (seconds) = \frac{Poling\ charge\ (Coulombs)}{Poling\ current\ (\frac{Coulombs}{second})}$$

The equation for the poling charge is given in the below equation. Q is the poling charge required, P_s is the spontaneous polarization constant (about 71 uC/cm^2 for LN), and A is the area of the poled region [8].

$$Q = 2P_sA$$

From the required charge and the poling current chosen from the circuit resistor design, the necessary pulse length is calculated. For the first LN experiments, this pulse length was found to be about 1 second.

Thus, the input waveform can be designed and implemented through the LabVIEW software and applied to the sample through the poling setup.

4. Testing

4.1 Probe Driving Distance

Once the LabVIEW software and poling setup designs were completed, the components were tested together. To ensure that the probes were making good contact with the sample during poling, the optimal driving distance was determined. The probes were driven different distances onto the same electrode pad, and the resistance across the probes was measured. Since the probes were touching the same pad, the resistance should ideally have been 0 Ω if there was good pad contact. Figure 8 on the next page is a plot of the measured resistance as a function of the drive distance. It shows that generally, the longer the drive distance, the smaller the resistance and the better the contact. However, the fact that there are multiple electrodes on one wafer sample prohibits drive distances longer than the distance between electrodes. As such, the best probe drive distance was chosen to be about 500 um, which is about the distance between electrodes. Figure 9 shows an image from the microscope of one electrode sample and the two probes.

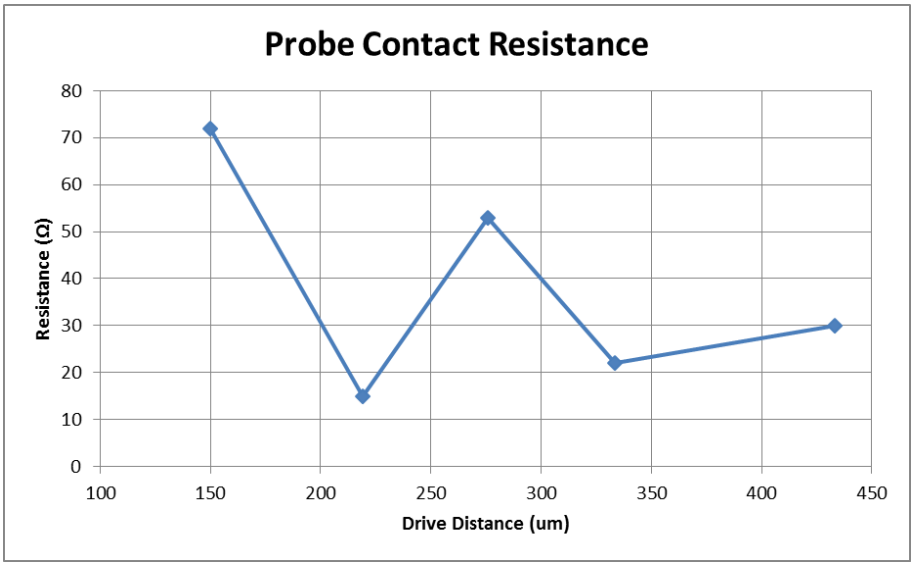

Figure 8: Plot of probe contact resistance as a function of driving distance.

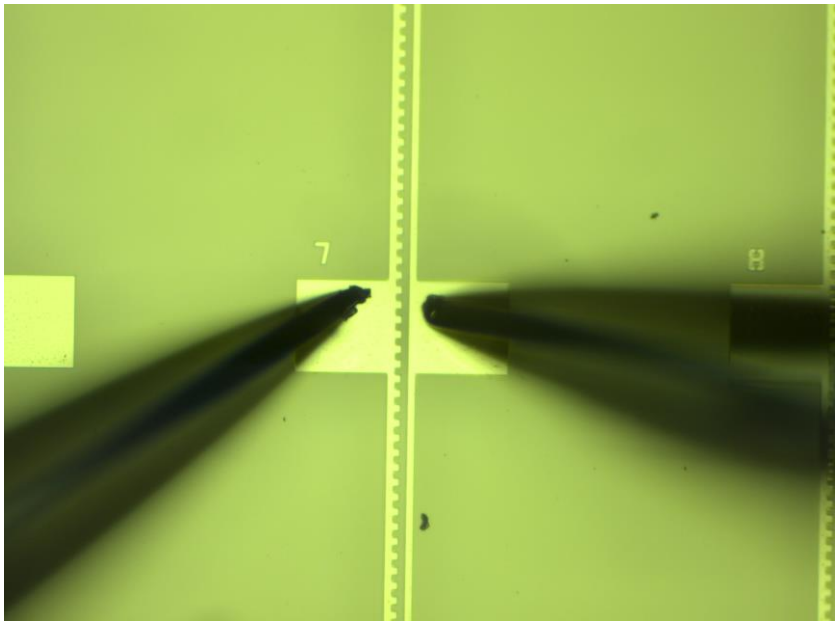

Figure 9: Microscope image of an electrode set with two probes. Note that the electrode on the left has a comb shape while the electrode on the right has a stripe shape.

4.2 Signal Noise

Initially, there was about a 60 Hz 0.125 Vpp sine noise signal on the V4 line on the oscilloscope when everything was connected and turned on. It was determined that the cause of the noise was coupling from other nearby cables (like the HVA cable and the wall outlet power cable). So, this issue was fixed by moving the cables far away from each other and wrapping some of the bigger ones in foil.

4.3 Breakdown Testing

Since the potential breakdown in the air between the probe needles was a safety concern, the first high-voltage tests with the poling setup were careful breakdown tests. The applied voltage to the circuit was slowly increased from 0 V to as high as 350 V by manually changing the AWG output by hand. The electrodes were monitored via the microscope camera to determine if breakdown occurred.

Paschen's law predicted that breakdown would have occurred between 300 V and 350 V for a 10 um air gap [14]. Nevertheless, no breakdown occurred as the voltage was increased. This verified that no oil bath was needed to prevent breakdown around the sample. The breakdown test also proved that the circuit and all equipment were able to handle the applied voltages required.

Although no breakdown occurred as the voltage was increased, some breakdown did occur on some electrodes for which the applied voltage was left on for an extended period of time. This showed what breakdown looked like. An image of one of the broken-down electrodes is Figure 10 on the next page.

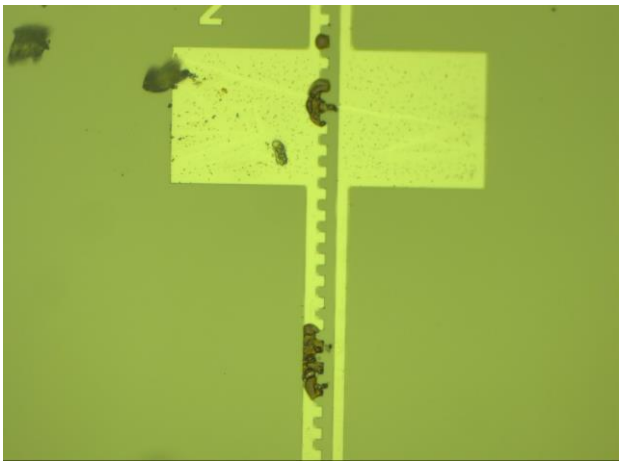

Figure 10: Microscope image of a broken down electrode. The dark splotches are the affected areas.

4.4 Open Circuit and Short Circuit Tests

During and after the breakdown testing, open circuits and short circuits were created for comparing the calculated and measured voltage values. The expected voltage values were determined with the MATLAB Poling Analysis script found in Appendix C, MATLAB Code. The voltage on the positive side of the sample, V2, was measured and calculated. The results of applying 250 V and 350 V to the system are shown in Table 1 below. The data show that the experimental open circuit and short circuit cases match very closely with the expected values calculated from MATLAB.

Table 1: Open circuit and short circuit test results.

Test	Expected V2	Measured V2
250 V Open Circuit	234 V	232 V
250 V Short Circuit	31.0 V	31.1 V
350 V Open Circuit	327 V	325 V
350 V Short Circuit	43.4 V	43.2 V

4.5 Initial Sample Tests

Once the circuit and MATLAB script were validated with the breakdown, open circuit, and short circuit tests, the actual LN sample was given a real poling waveform. However, when the sample was inserted, the measured V3 voltage was much smaller than expected. On the order of 10s of mV were measured, and the MATLAB script predicted V3 on the order of 10 V. The low V3 possibly indicated a lack of poling current.

Thus, this big difference in V3 was a concern and led to many attempted fixes. Different electrodes were tried with the same waveforms. The probes were moved as close to each other as possible while still being on separate pads. Electrodes were poled for longer periods of time and more individual times in a row. The positive and negative probes were swapped in case of a polarity problem. The max voltage was increased to 400 V. The voltage across the probes was measured directly to determine if the voltage measured at the circuit was the same as on the sample, and it was. All of these tests led to the same low V3 issue.

However, when a whole new wafer sample of electrodes was tried with a fresh start, some patterns began to emerge in the testing. Even though the V3 voltage was still smaller than predicted, it was realized that the shape of the V3 wave matched the expected shape. Three examples of the V3 wave shape are shown in Figure 11 on the next page. All three images show that soon after the applied voltage reached the coercive field voltage, the pink V3 line spiked up from nothing to a steady value. Three different poling waveforms were used, and the voltage spike occurred for each input. This voltage spike was expected and matched the responses seen in the literature [15]. The discovery of the pattern of the correct poling wave shape for V3 helped determined that poling was likely actually occurring even though the measured current amplitude did not match.

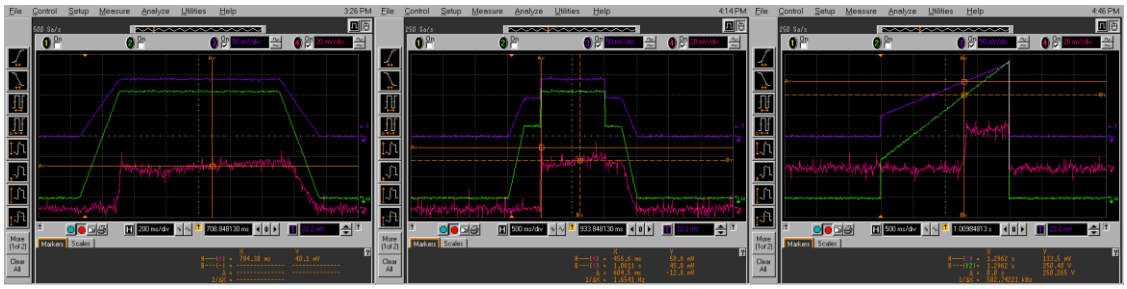

Figure 11: Three example test waveforms. The input waveforms are in purple. The voltages on the positive side of the sample are in green. The pink lines represent the voltage on the negative side of the sample, or the poling current. Note that the pink poling current lines all spike up at a point when the positive voltage surpasses the coercive voltage.

5. Baseline Poling Results and Characterization

5.1 Parameter Sweeping

Once it was determined that actual poling was likely occurring during the poling tests, the next step was to perform a parameter sweep on multiple electrodes. This was to be able to evaluate the extent of the poling and determine the best combination of the variables after characterization.

A total of 16 electrodes were poled in the parameter sweep in order to vary: electrode length, poling period, waveform voltage, and waveform duration. Firstly, the electrodes were either long or short in length, and the short ones were also symmetrical in that they had combs on both sides instead of one comb and one strip. Secondly, the poling periods were 3.7 um and 20 um. Thirdly, the waveform voltages were 250 V and 300 V. Both voltages were above the coercive voltage of about 210 V. Fourthly, the waveform durations were 1 second and 3 seconds.

During the poling, most of the electrodes displayed the same current spike (in terms of voltage V3) as seen during the tests. This was an initial indication that the poling was working. However, there were a few combinations of variables which did not seem to work properly

during poling. Specifically, some of the short, symmetrical electrodes seemed to break down at the higher voltage or the longer duration. So, these electrodes were immediately excluded from any characterization processes.

5.2 FIB Milling and HF Etching

Four of the poled electrodes which showed expected voltages on the oscilloscope were chosen for characterization to be able to see how well the poling occurred. The traditional process is to use focused ion beam (FIB) milling and hydrofluoric acid (HF) etching [4]. FIB milling shoots ions onto the surface of the poled sample to remove the copper metal electrodes. This allows for the HF etching to reveal the physical ridges associated with poling.

FIB milling and HF etching were done on the four poled electrode samples. The FIB milling was done in a way to keep some of the copper electrodes visible for locating the poled regions upon examination. The HF etching was done for cumulative 20 minutes, 35 minutes, and 55 minutes, but the resulting images reached the best quality around 35 minutes of etching. Images were taken using the FIB, optically, and using a scanning electron microscope (SEM).

From the resulting HF etching images, it can be seen that some degree of poling had indeed occurred. The best SEM image showing this poling is shown in Figure 12 on the following page. This electrode with the best baseline poling results was a long electrode with period 3.7 um that was given 250 V for 1 second. Figure 12 shows remnants of the comb electrodes on the bottom of the image. From the “fingers”, one can see streaks of darker-colored material spreading to the other strip electrode. These dark streaks represent the flipping of the domains along those paths and verify the success of baseline poling.

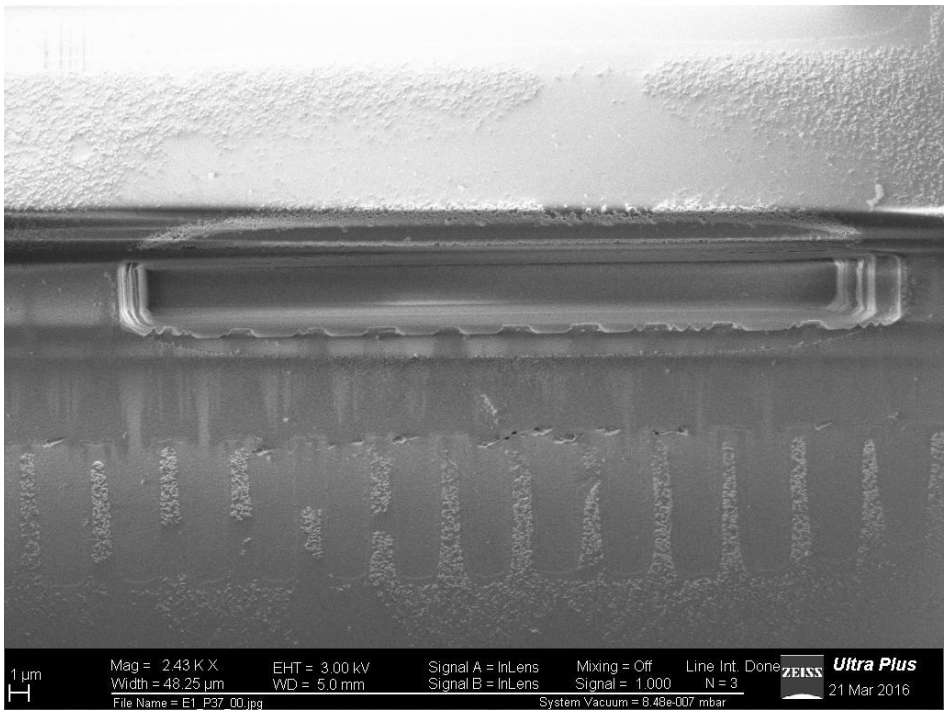

Figure 12: Best result of HF etching of the baseline LN poling. Parts of the poling electrodes remained and can be seen. The dark streaks reaching from the electrode comb remnants represent the successful domain inversion poling.

Even though this result proved that the baseline poling succeeded, the images also showed that there was room for optimization. Firstly, the poling streaks were not uniform along the whole electrode. This could indicate that the poling parameters were not ideal. Secondly, the streaks spread wider than the electrode fingers' width, which should not occur. This indicates that the sample may have been over-poled, allowing for the domains to grow too much [16]. Since the nonlinear optical processes using the poled sample will be designed assuming a 50% duty cycle, it was important to attempt to optimize the poling quality to increase uniformity and fine-tune domain growth for further poling.

Additionally, these methods of characterization are destructive to the poled samples and are not ideal for verifying a usable sample. This motivated the search for another, non-destructive way to characterize the poling.

5.3 PFM

Piezoresponse force microscopy (PFM) is a non-destructive method for imaging the ferroelectric domains of a sample. PFM works by applying an AC voltage to the sample and measuring the expansion and contraction of the sample with a cantilever probe [17]. The sample experiences physical deflections due to the piezoelectric effect.

Conveniently, it was determined that PFM was capable of detecting deflections even in x-cut materials [17]. The concern was that x-cut materials would not react to the applied voltage with any out-of-plane (z-direction) movement. However, the movement in the x- and y-directions are detected as torsion or buckling [17]. The PFM is able to measure this torsion by the cantilever's vertical displacement. Torsion will occur for periodically poled samples because the domains are re-oriented to a certain in-plane direction. Figure 13 below shows the basic cantilever movements and forces for the PFM.

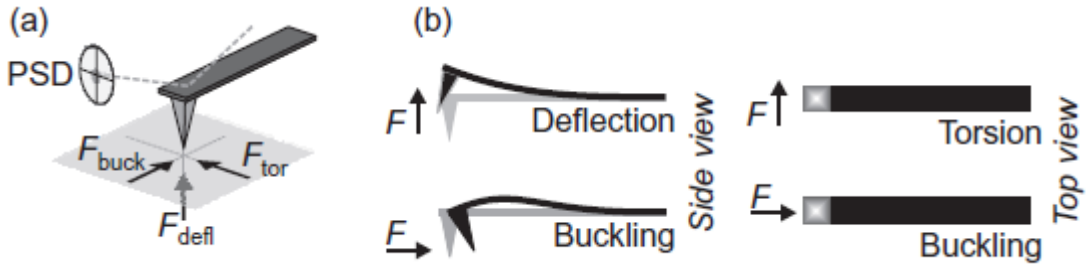

Figure 13: Basic PFM cantilever movements which allow for characterizing x-cut poling. [17]

Since PFM involves just applying a voltage and measuring deflection, it is a non-destructive method for verifying the poling success and analyzing its quality. It is also relatively faster than going through the full FIB milling and HF etching process. The PFM amplitude image of the best quality poled electrode is shown in Figure 14 on the next page. This figure

shows a very similar pattern to the previous HF etching image. The domain poling can be seen as the dark brown streaks, and the same lack of optimization is noticed. However, the advantages in speed and non-destructiveness are valuable, and PFM will be used for further poling characterization.

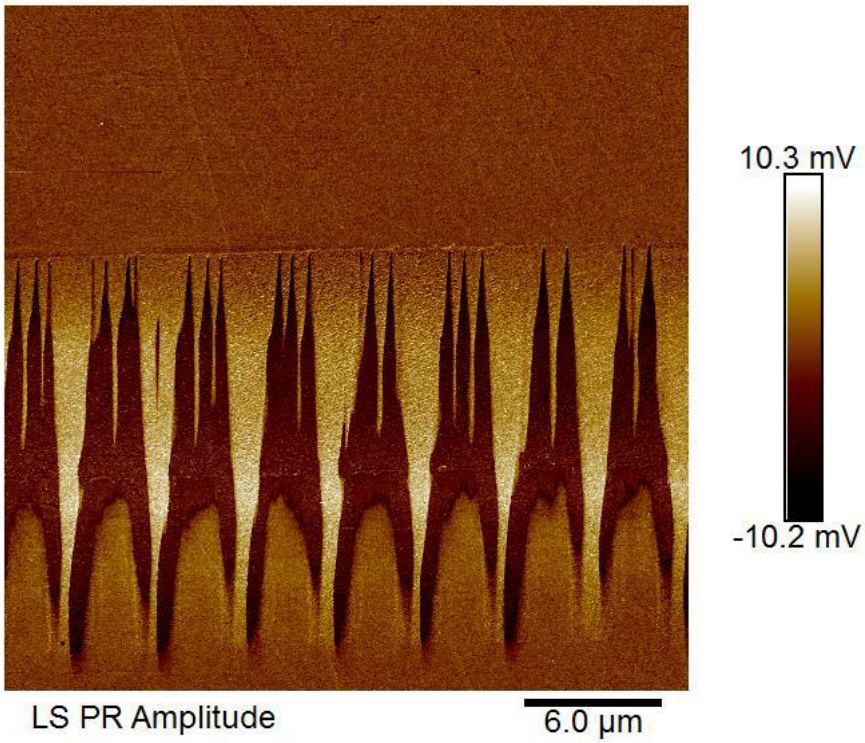

Figure 14: Best PFM poling results. This graph shows the cantilever amplitude response, which is different for differently polarized regions. Thus, the darker spiky regions growing from the bottom comb to the top strip represent the successful domain inversion.

6. Changes for MgO:LN Poling

6.1 MgO-Doped LN Parameters

MgO:LN wafers were then used because of the smaller coercive field strength required for poling and the lesser tendency toward photorefractive damage [15]. These lead toward the goal of on-chip dynamic poling because the smaller the required voltage, the easier it is to

generate that voltage on a chip. Because of the smaller coercive field strength and different spontaneous polarization constant, the poling waveform and circuit resistors needed to change.

The exact coercive field strength of the MgO:LN was not given by the vendor. So, a ramp waveform test was conducted to determine experimentally the coercive voltage needed [13]. The prepared sample was put in the holder, and the probes were connected to the electrode pads. Then, a ramp input wave from 0 V to 200 V was applied to the sample. The input wave and the resulting V2, V3, and Vc=V2-V3 voltages are shown in Figure 15 below. The figure shows that the voltage Vc across the sample did indeed clamp at a voltage of about 105 V. This occurred at an input voltage of about 150 V and generated about 11 V of V3. These values approximately matched the values predicted by the MATLAB Poling Analysis script.

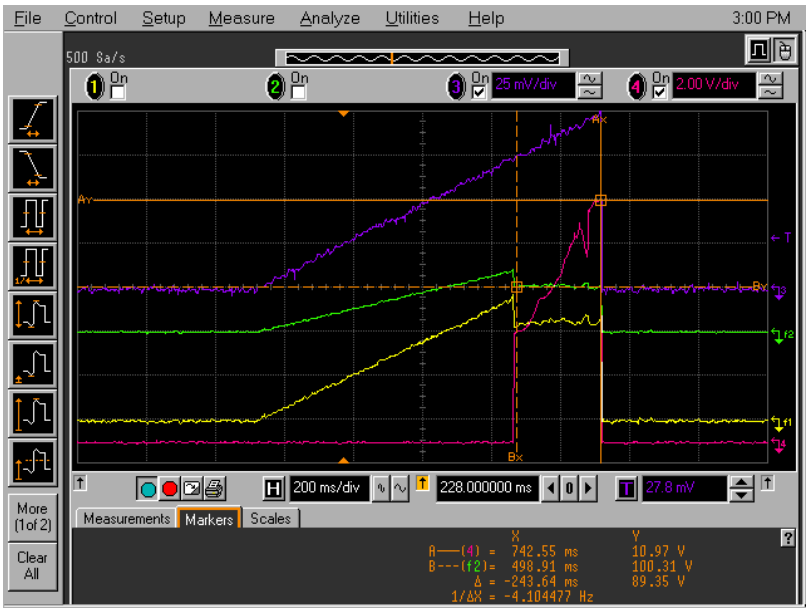

Figure 15: Ramp wave input test results used to determine the approximate coercive field voltage of the MgO:LN sample. The purple line is the input voltage, the yellow line is V2, the green line is the voltage across the sample, and the pink line is V3, the poling current. Note that the current jumps as soon as the voltage across the sample clamps, as expected.

From the ramp wave voltage data and the original resistors in the circuit, the poling current for an input of about 150 V was calculated to be about 34 uA, which was on the expected order of magnitude. The calculated poling charge was calculated as $Q = 3.535 \times 10^{-4}\ uC$. From the current and charge, the required pulse length was then calculated as only about 10 us.

The required pulse length of only 10 us raised again the issue of rise time of the HVA. It was previously determined that the HVA cannot respond quickly to even a 1 ms pulse, as shown in Figure 16 below. When a 10 us pulse was sent through the HVA, it did not even turn on the HVA before the end of the pulse. From sending more pulses, it was determined that a pulse length of 10 ms was the shortest acceptable length due to the minimal rounding of the HVA response, as shown in Figure 16. However, increasing the applied pulse length decreases the poling current obtained, which makes it more difficult to measure the voltage V3 on the oscilloscope during poling.

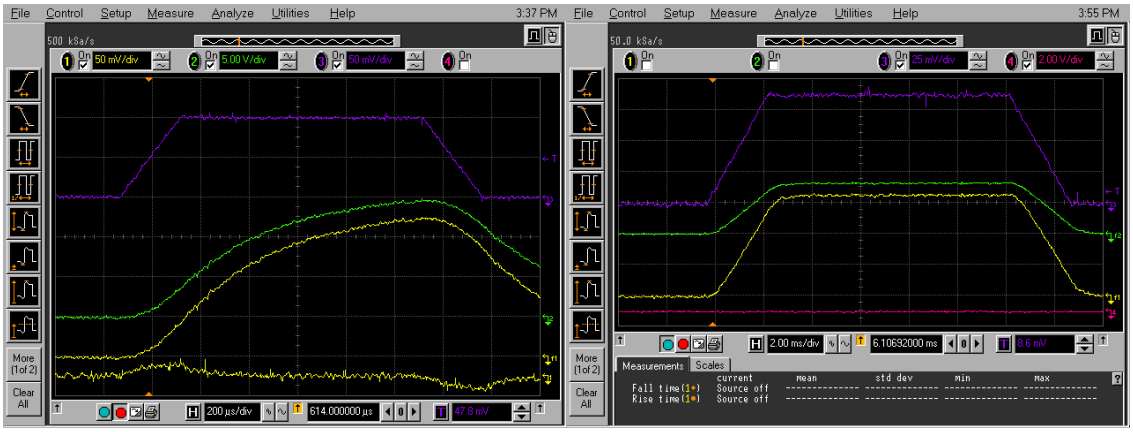

Figure 16: Short pulse duration results. The left shows a 1 ms pulse to which the HVA cannot respond quickly enough. The right shows a 10 ms pulse to which the HVA was deemed to respond just well enough.

In order to increase the waveform duration so that the HVA can respond quickly enough but also keep V3 high enough to measure, the MATLAB Poling Analysis script was used to tune the poling circuit resistor values. A balance between pulse length and expected V3 was sought. This involved changing the value of the resistor R1 to change the poling current and the waveform length and then changing the resistor R4 to increase the measured V3. The selected values led to expected pulse length of about 100 ms and expected V3 measured of about 50 mV.

6.2 Poling Circuit Design Improvement

Since the change to using MgO-doped LN led to the need to change the circuit resistor values, the circuit setup design was improved, as well. In order to allow for more easily changing the resistors in future experiments for potentially different materials, the permanent soldering and heat shrink tubing of the resistors and cables was undone. Instead, a breadboard was implemented to allow for easy replacement of resistors. A small project box was prepared so that the breadboard and open wires would be closed off from people. Only the input HVA power and ground cables and the positive and negative sample probes have input connections. The output connections are restricted to just the measured voltages for the oscilloscope (V4 and V3 and ground). Figure B4 in Appendix B, Poling Setup Pictures, shows the circuit project box.

After making this setup change, about 20 mV of noise was noticed on the V4 and V3 lines with the oscilloscope. Since V3 was to be on the order of mV, the noise needed to be reduced to be able to measure V3 and thus know the poling current. This reduction was achieved by moving the power cables as far away from the circuit and oscilloscope probes as possible. Also, the circuit box was wrapped in foil to further prevent coupling of signals.

7. MgO:LN Poling Results and Characterization

Despite the theoretically optimized pulse length and measurable poling current values from choosing new resistors, no visible poling was achieved with the MgO:LN. In the initial poling tests, appropriate V3 voltages were measured, indicating a presence of poling current. However, using PFM to characterize the poling showed no changes from before poling. It was discovered that one way to explain this development of current without poling was the presence of a lot of leakage current [15, 18]. This leakage current was not an issue with the baseline LN because the MgO-doped LN experiences more random domain growth during poling. This random domain growth causes some poled regions to draw current first, which then reduces the strength of the applied electric field across the gap. If the field reduces too much, then it is under the coercive field required for continued poling, and no poling remains [18]. Two ways described in the literature to get around this problem with MgO:LN are to: increase the pulse length by a large factor to force more of the sample to become poled [18] or pole the sample with lots of small pulses [19]. These two methods were attempted with the MgO:LN samples, but still the current showed up without any poling results via PFM.

8. Conclusion

A dynamic periodic poling system was designed and tested for poling x-cut LN and MgO:LN. The LabVIEW control software allows for easy waveform creation and sending the applied waveform through the AWG and into the HVA. Many different kinds of waveforms can be created, saved, and recalled for different poling needs. The poling circuit setup allows for easy replacement of resistors to change parameters such as the input pulse length and total charge on the sample. With the software and instrumentation setup, many poling tests were conducted for

baseline LN poling. After refining the setup and waveform, the baseline poling was achieved and characterized with FIB milling and HF etching. Additionally, PFM was used as a non-destructive and more efficient method of characterization. Despite the changes made to accommodate MgO-doped LN, poling was not achieved for this sample. One potential issue with poling MgO:LN is the increased amount of leakage current, which was difficult to overcome. Nevertheless, the created periodic poling system was successful in achieving baseline poling of x-cut LN for use in on-chip integrated optics and in laying the foundation for poling of other materials with different nonlinear optical properties.

9. Future Work

The main area for improvement of this periodic poling system is in being able to pole the MgO:LN sample. This will involve further investigation into the properties of doped LN as well as the amount of leakage current observed. One possible solution to this problem is to use an off-axis substrate when poling [18]. This would prevent random domain growth from reaching the other side of the poling gap and causing premature leakage current [18].

In addition, there are two farther-out goals of the poling system: being able to pole thin films on-chip, and being able to reverse pole a sample back to its original polarization. These lead toward the idea of dynamic on-chip poling of a material such that an optical circuit could physically change simply by applying a voltage to pole, reverse pole, and pole again. Thin film poling is more difficult than bulk poling due to the higher electric fields needed, but is starting to become possible especially due to the successes in x-cut poling [19]. Reverse poling may be similar to hysteretic ferroelectric memory [20]. Both of these are potential future endeavors.

10. References

[1] R. W. Boyd, *Nonlinear Optics*, 3rd Edition, 2008

[2] S. Smith, "Investigation of nanoscale etching and poling of lithium niobate", Montana State University, 2014

[3] V. Shur, "Nanoscale backswitched domain patterning in lithium niobate", Applied Physics Letters, vol. 76, 2000

[4] G. Miller, "Periodically poled lithium niobate: modeling, fabrication, and nonlinear-optical performance", Stanford University, 1998

[5] P. Mackwitz, "periodic domain inversion in x-cut single-crystal lithium niobate thin film", Applied Physics Letters 108, 2016

[6] TREK Model 20/20C High-Voltage Power Amplifier Manual

[7] K. Nakamura, "Periodic poling of magnesium-oxide-doped lithium niobate", Journal of Applied Physics, Volume 91, Number 7, 2002

[8] L. E. Myers, "Quasi-phase-matched optical parametric oscillators in bulk periodically poled $LiNbO_3$", J. Opt. Soc. Am., B/Vol 12, No. 11, 1995

[9] A. Kaul, "Fabrication of periodically poled lithium niobate chips for optical parametric oscillators", Pramana Journal of Physics, Vol. 75, No. 5, 2010

[10] Stanford Research Systems Arbitrary Waveform Generator Software AWC

[11] Stanford Research Systems DS345 Arbitrary Waveform Generator Manual

[12] R. G. Batchko, "Domain patterning in lithium niobate using spontaneous backstitching", Stanford University, 1999

[13] B. F. Johnston, "Fabrication and characterization of poled ferroelectric optical crystals", MQ Photonics Research Centre, 2008

[14] L. F. Berzak, “Paschen’s law in air and noble gases”, 2006

[15] S. Sonoda, “Second harmonic generation in electric poled x-cut MgO-doped $LiNbO_3$ waveguides”, Miyanodai Technology Development Center, 1997

[16] A. C. Busacca, “Surface domain engineering in congruent lithium niobate single crystals: A route to submicron periodic poling”, Applied Physics Letters 81, 2002

[17] T. Jungk, “Contrast mechanisms for the detection of ferroelectric domains with scanning force microscopy”, New Journal of Physics 11, 2009

[18] K. Mizuuchi, “Electric-field poling in Mg-doped $LiNbO_3$”, Journal of Applied Physics 96, 2004

[19] L. Chang, “Thin film wavelength converters for photonic integrated circuits”, Optica, Vol. 3, No. 5, 2016

[20] G. J. M. Dormans, “Pulse measurements on ferroelectric capacitors simulating memory switching”, Applied Physics Letters 65, 1994

Appendix A

Poling Setup Materials

Table A1: List of all poling setup equipment, quantity, and vendor, as appropriate.

Item	Quantity	Vendor
SRS DS345 Synthesized Function Generator	1	Stanford Research Systems
NI GPIB-USB-HS Controller	1	National Instruments
HP Infinium Oscilloscope	1	Hewlett Packard
10:1 Oscilloscope Probes	2	Hewlett Packard
TREK 20/20C High-Voltage Power Amplifier	1	TREK
HVA Cable	1	TREK
Laptop	1	N/A
Power Strip	1	N/A
Cart	1	N/A
Microscope	1	N/A
Keithley 7078-TRX-10	1	Newark element14
Keithley 237-TRX-BAR	2	Mouser Electronics
Probe Arm PH120	2	Suss MicroTec
SEMCLIP Clips, PKG/10	1	Ted Pella
Screws, Brass M2X3, PKG/10	1	Ted Pella
Sample Dish	1	N/A
1.5” Mounting Post Bracket	2	ThorLabs
1.5” Mounting Post, L=14”	2	ThorLabs
Stainless Steel Custom Mounts	2	In House
1/8 W Resistors	4	N/A
Breadboard	1	Radio Shack
Project Box	1	Radio Shack

Appendix B

Poling Setup Pictures

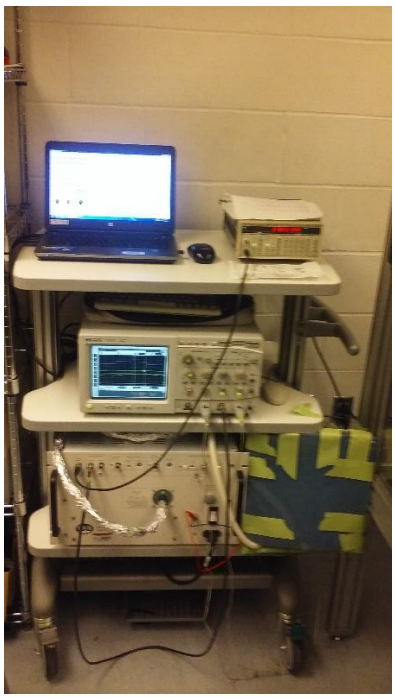

Figure B1: Poling control cart. Top shelf: laptop and Arbitrary Waveform Generator. Middle shelf: oscilloscope. Bottom shelf: High-Voltage Amplifier and covered poling circuit box.

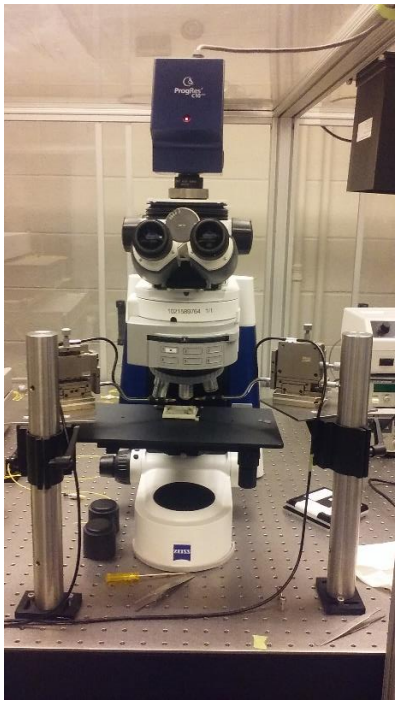

Figure B2: Poling sample station. The sample holder is on top of the stand of the microscope. To each side is a post with a steel stand for a DC probe.

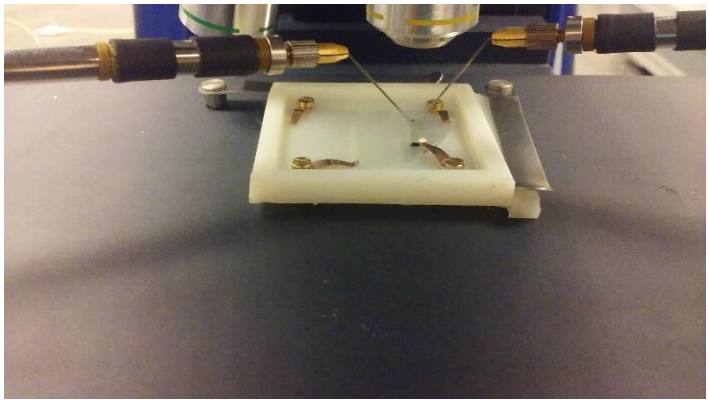

Figure B3: Up-close picture of the sample holder with the LN sample inside. The clips hold the sample in place, and the probes contact the sample on specific electrodes. The microscope is used to accurately place the probes.

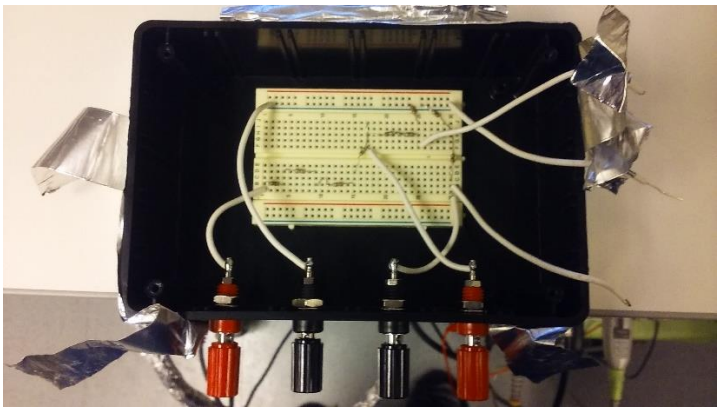

Figure B4: Poling circuit project box. The circuit resistors are placed on a breadboard for easy replacement. The four jacks in the bottom of the picture are for the HVA voltage, HVA ground, negative probe, and positive probe, from left to right. The three wires on the right are for the oscilloscope measurement probes and represent V4, ground, and V3, according to the poling circuit in Figure 5.

Appendix C

MATLAB Code

MATLAB Poling Circuit Analysis Code:

```
clear;
clc;

% Define all inputs and parameters
Vc=85;
V1=200;
R1=22.68e6;
R2=20.22e6;
R3=2.28e6;
R4=20.01e6;
R_probe = 10e6;
R3_eff=(R3*R_probe)/(R3+R_probe);
R4_eff=(R4*R_probe)/(R4+R_probe);
Rp=R2+R3_eff; % Total votlage divider resistance
Rt=(Rp*R4_eff)/(Rp+R4_eff) + R1; % Total

% Open circuit case (before poling current)
I=V1/(R1+R2+R3_eff);
V2=V1-I*R1
R1_power_open=I^2*R1

% Normal operation
V2_norm=(V1/R1 + Vc/R4_eff)/(1/R4_eff+1/R1+1/Rp) % With voltage
divider
V3_norm=V2_norm-Vc
V4_norm= V2_norm*R3_eff/(R2+R3_eff)
I_poling=V3_norm/R4_eff

% Short circuit case
I1_short= V1/Rt
V3_short= V1-I1_short*R1
V4_short= V3_short*R3_eff/(R2+R3_eff)
V2_short= V3_short
R1_power_short = I1_short^2*R1 % Check power across resistors
for safety

% Charge and pulse length
Qlong = 2*3.535E-10; % In Coulombs
PulseLength = Qlong/I_poling % In seconds
```

Appendix D

LabVIEW Code

LabVIEW Poling Software Block Diagram Code:

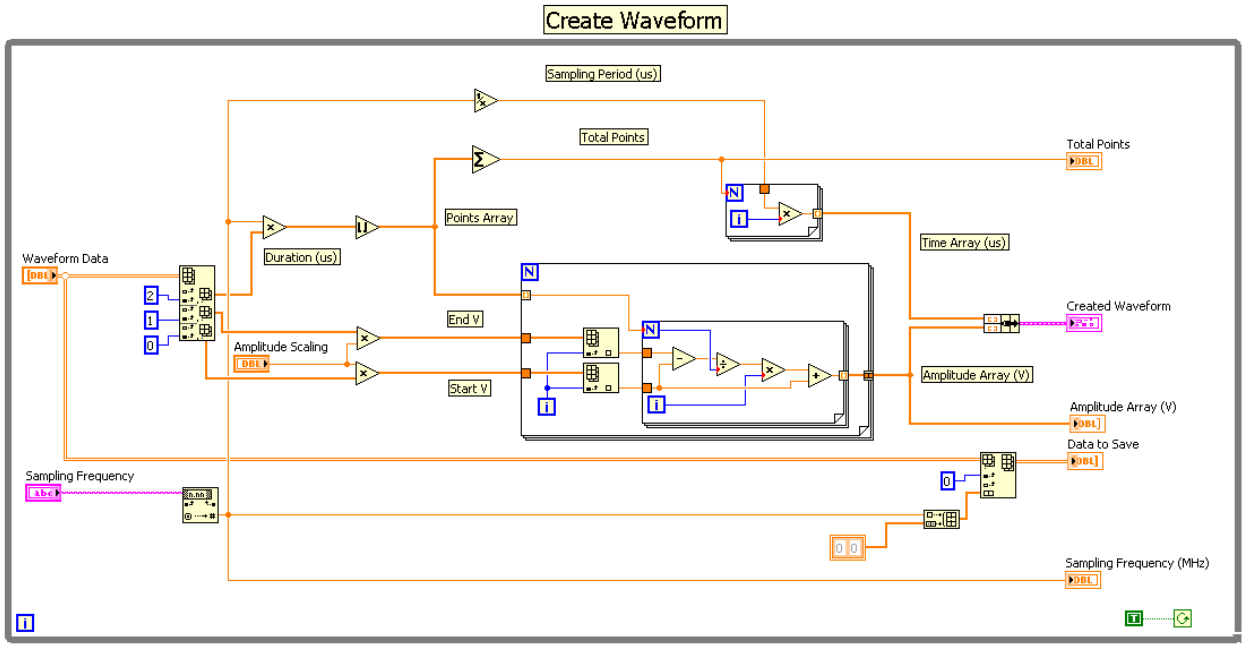

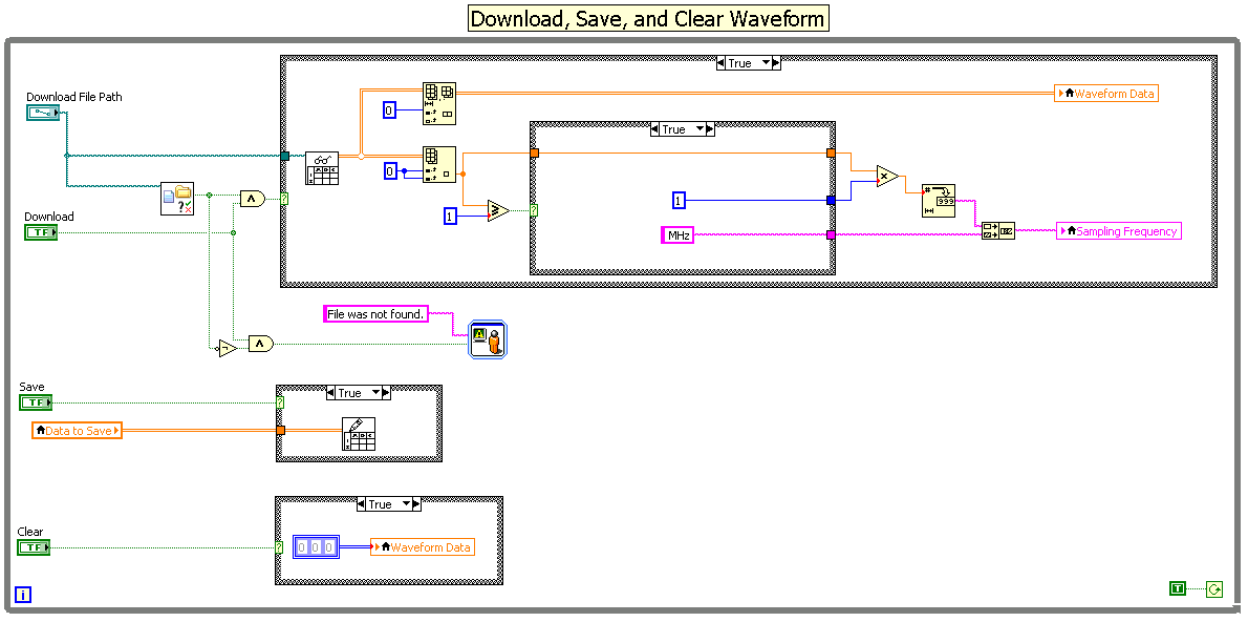

Prepare and Send Data Over GPIB

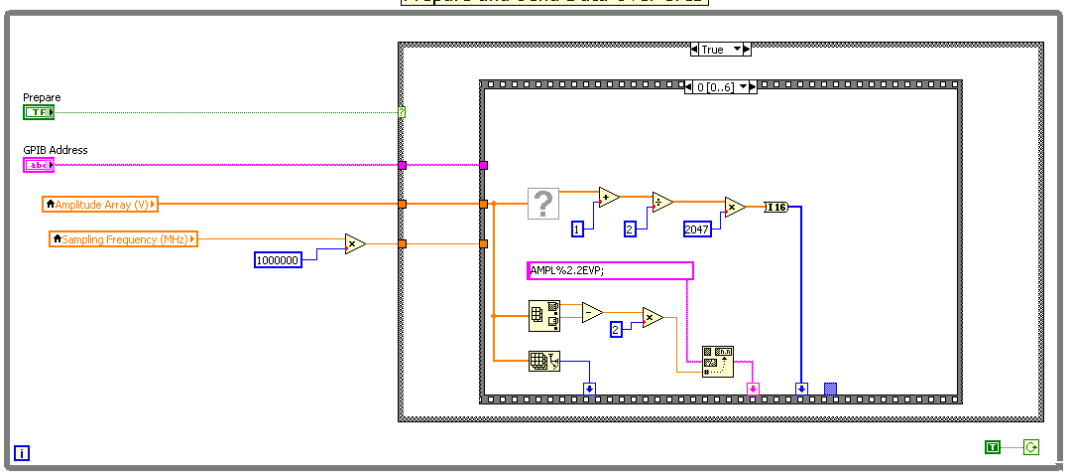

Open Manual PDF

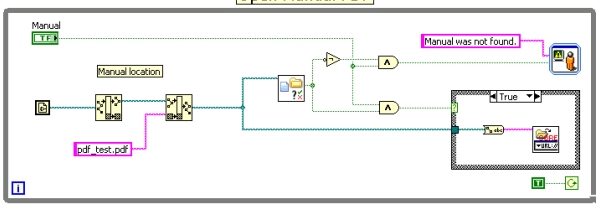

Initialization

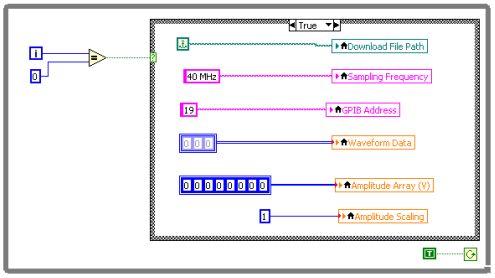

Error Checking